Title
DEVELOPMENT OF A LI[SUP]- ION SOURCE

Authors
Walther, S.R.
Morse, E.C.
Leung, K.N.

Publication Date
1989-02-01

LBL-26757
Preprint

Lawrence Berkeley Laboratory
UNIVERSITY OF CALIFORNIA

Accelerator & Fusion
Research Division

Submitted to Journal of Applied Physics

Development of a Li^- Ion Source

S.R. Walther, E.C. Morse, and K.N. Leung

February 1989

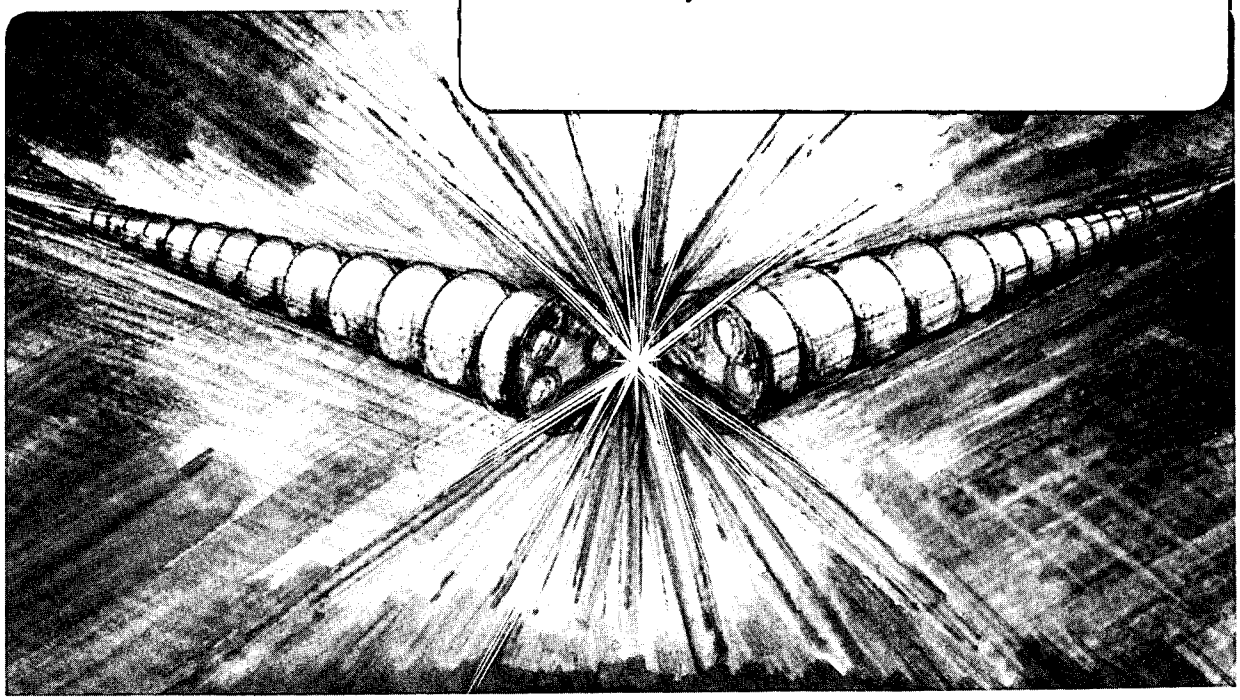

Prepared for the U.S. Department of Energy under Contract Number DE-AC03-76SF00098.

DISCLAIMER

LBL-26757

DEVELOPMENT OF A LI⁻ ION SOURCE*

S.R. Walther,[Π] E.C. Morse,[Π] and K.N. Leung

Accelerator and Fusion Research Division
Lawrence Berkeley Laboratory
#1 Cyclotron Road
Berkeley, CA 94720

* This work is supported by the AFOSR (under Contract No. AFOSR-ISSA-88-033), and the Director, Office of Energy Research, Office of Fusion Energy, Development and Technology Division, of the U.S. Department of Energy under Contract No. DE-AC03-76SF00098.

Π Also with the Nuclear Engineering Department, University of California, Berkeley, CA.

Development of a Li^- Ion Source*

S. R. Walther†, E. C. Morse†, and K. N. Leung

Accelerator and Fusion Research Division
Lawrence Berkeley Laboratory
1 Cyclotron Road
Berkeley, CA 94720

Abstract

Sources of Li^- ions are needed for diagnostic neutral beams for fusion research. Previous efforts to generate Li^- beams have focused on electron capture in a gas or production on a low work function surface in a plasma. Volume production of Li^- by dissociative attachment of optically pumped lithium molecules has also been studied. This paper presents experimental results for volume production of a Li^- ion beam from a plasma discharge. These results show that a discharge source of Li^- ions can provide suitable current densities for diagnostic beams. A theoretical model for the formation of Li^- ions from Li_2 molecules in the lithium discharge is developed. The model is in good agreement with the experimental results and shows favorable parameter scalings for further improvement of the Li^- ion source.

*This work is supported by the AFOSR (under Contract No. AFOSR-ISSA-88-003), and the Director, Office of Energy Research, Office of Fusion Energy, Development and Technology Division, of the U.S. Department of Energy under Contract No. DE-AC03-76SF00098.

†also with the Nuclear Engineering Department, University of California at Berkeley.

INTRODUCTION

Sources of Li^- ions are needed to generate efficient neutral beams with energies in excess of 150 keV per nucleon for fusion research.[1] Fusion plasma diagnostics using Li^- ions to generate high energy neutral beams of Li° with energies of .5 to 5 MeV have been proposed.[2,3] Diagnostic uses for lithium beams include in situ measurements of magnetic field, magnetic pitch angle, and current density in a tokamak. These measurements have already been demonstrated on the Texas EXperimental Tokamak (TEXT) with a positive ion based system at low energies (~100 keV).[4,5] If such a system were implemented on a large tokamak, such as ITER, beam energies of 1 to 2 MeV per nucleon would be desirable.[6] It has also been proposed to use a neutral lithium beam to measure the velocity distribution of fast confined fusion alpha particles.[2] Therefore the development of Li^- ion sources is of considerable interest for fusion applications.

A great deal of work has been devoted to H^- (D^-) ion source development and the relevant atomic processes. Due to the similarity of the H^- and Li^- systems, it will be assumed that the relevant H^- atomic physics can be adapted to the Li^- system. An important difference is the ratio of atoms to molecules in the ion source. In a H^- ion source, H atoms are assumed to be a small but important fraction of the neutral species. In a Li^- ion source, it is the Li_2 molecules which are in the minority, because of the small binding energy of the Li_2 molecules (1.06 eV). The dimer molecules are important, since H^- and Li^- ions are believed to be formed in the volume predominantly by dissociative attachment:[7,8,9,10]

$$H_2(v^*) + e^- \rightarrow H + H^-, \qquad (1)$$

$$Li_2(v^*) + e^- \rightarrow Li + Li^-, \qquad (2)$$

where $X(v^*)$ denotes a vibrationally excited molecule. The lack of Li_2 molecules in equilibrium makes Li^- production difficult. Nonequilibrium situations, such as supersonic expansion through a nozzle, can be used to increase the dimer fraction in a Li^- ion source, however.

I. ION SOURCE DESIGN AND OPERATION

A successful preliminary investigation of volume Li^- production in a plasma discharge has been reported previously.[11] In this report, these results are expanded upon with further experiments and a model for ion source operation. An alternative approach, volume production of Li^- ions by optically exciting high vibrational states in Li_2 molecules, which subsequently dissociatively attach to low energy electrons produced by photoionization, has been demonstrated by McGeoch and Schlier.[12] However, it is generally more economical to produce Li^- ions in a discharge, since the efficiency of electron impact excitation or ionization can be much higher than that of corresponding photon processes. Demonstration of current densities in the mA/cm^2 range would be required for diagnostic purposes, and the experiments described here show that this is feasible.

The ion source is constructed of a cylindrical water-cooled copper chamber (2.5 cm diameter by 5 cm long) with the open end enclosed by a two-grid ion extraction system. A schematic diagram of the ion source is displayed in Fig. 1. The source chamber is surrounded externally by 16 columns of ceramic magnets to form a longitudinal line-cusp configuration for primary-electron and plasma confinement. The use of 16

columns, as opposed to a smaller number, allows a larger 'field-free' region (B < 10 G) where the filament is placed and primary electrons are emitted. The magnet columns on the cylindrical wall are connected at the end flange by two rows of samarium cobalt magnets that are also in a line-cusp configuration.

A samarium cobalt magnetic filter near the plane of extraction and external to the ion source divides the chamber into an arc discharge and an extraction region (i.e. a 'tandem discharge'). The filter magnets provide a transverse magnetic field (B = 250 G at the center), which serves to prevent energetic primary electrons from reaching the extraction region. However, positive ions, negative ions, and low energy electrons can diffuse across the filter into the extraction region to form a plasma there. The length of the extraction region from the plasma electrode to the center of the filter field is approximately 4 mm.

Inside the source chamber is a heat shield constructed of molybdenum sheet metal (7.6×10^{-3} cm thick), which forms the wall surface. Initial experiments used solid lithium placed in the discharge chamber as the source of lithium vapor for the discharge. A lithium discharge was initiated by using a low power argon discharge to heat the ion source wall, which evaporated some of the lithium. A local hot spot is initially produced by the lithium sample, since it sticks into the plasma and is preferentially heated relative to the rest of the ion source wall. Once in the vapor phase, lithium completely dominated the ion species in the discharge and the argon gas was removed. Although a pure lithium discharge can be achieved in this manner, there is a time dependence to the neutral density in the ion source. Lithium vapor can escape through the extraction aperture and leave the ion source, or find a cold spot on the

ion source wall and condense in solid form. Thus, the neutral lithium density in the source will decrease with time.

A two-electrode acceleration system is attached to the open end of the chamber. The extraction aperture is 1 mm in diameter giving an extraction area of 7.85×10^{-3} cm^2. The source and the first or plasma electrode are biased negative for negative ion extraction and positive for positive ion extraction. The second electrode is electrically grounded. A plasma is produced by primary electrons emitted by a 0.5-mm-diameter hairpin tungsten filament. The chamber wall, heat shield, and plasma electrode serve as the anode for the discharge.

Located downstream from the second electrode is a compact magnetic deflection spectrometer[13] for measurement of the positive or negative ion species in the extracted beam. In order to measure the negative ion current, the electrons in the extracted beam are removed with a permanent magnet mass separator,[14] which generates a B field strong enough to remove electrons but does not perturb the ion trajectories significantly. The electrons are collected on ridged graphite plates in the mass separator and the current is measured. The remaining beam, composed solely of negative ions, is collected in a Faraday cup. This arrangement, schematically represented in Fig. 1, provides the total negative ion current and the ratio of extracted electrons to negative ions.

II. EXPERIMENTAL MEASUREMENTS FOR DISCHARGE EVAPORATION OF LITHIUM

A. Dimer Fraction in the Discharge

The ion source was operated with an arc voltage of 40 V and an arc current of 4 A as typical discharge parameters. The mass spectrometer

was used to measure both the positive and negative extracted ion species. Fig. 2(a) shows the mass spectrometer output signal for the positive extracted ion beam. $^6Li^+$, $^7Li^+$, and Li_2^+ are present in the beam, with $^7Li^+$ composing ~81% of the beam current. The small peak at mass 13 is presumably Li_2^+ ions formed by the combination of ^6Li and ^7Li atoms. The ratio of $^6Li^+$ to $^7Li^+$ ions is exactly that of the natural isotopic mix of lithium.

Using this information, the dimer fraction in the ion source can be estimated. Li_2^+ ions compose ~12.3% of the total lithium positive ion current. To calculate the corresponding ion fraction in the ion source, the velocity difference between atomic and molecular ions must be taken into account. In an ion source with a positive plasma potential such as this one, ions reach the extractor with the ion acoustic speed. The ion acoustic speed is inversely proportional to the square root of the ion mass, therefore Li_2^+ ions have a velocity that is $2^{-1/2}$ that of $^7Li^+$. Hence the percentage of Li_2^+ ions in the ion source is ~18.4%. To infer the neutral species ratio from this, the difference of ionization cross sections must be accounted for. Unfortunately, the electron impact ionization cross section for Li_2 is not known. However, an estimate can be made using hydrogen data, since only the ratio of the atomic to molecular ionization cross section is needed. The lithium discharge is characterized by 40 eV primary electrons, which perform most of the ionization. To translate this to the hydrogen system, a corresponding electron energy is given by 40 eV multiplied by the ratio of hydrogen to lithium ionization energies (13.6/5.4), giving an electron energy of ~100 eV. For an electron energy of 100 eV, the ratio of atomic to molecular hydrogen ionization cross sections is ~0.67.[15] Hence, to infer the

percentage of Li_2 in the neutral species of the discharge the percentage of molecular ions (18.4) must be corrected for the larger ionization cross section of the molecules relative to the atoms (~0.67). This gives a value of 12.3% as the percentage of Li_2 in the neutral species in the ion source. The preceding calculation is subject to some error due to the use of the hydrogen data to determine the lithium ionization cross section ratio, but this error should not be too large because other atomic/molecular systems have similar cross section ratios (0.56 for nitrogen, 0.57 for oxygen).[15]

B. Neutral Lithium Density in the Ion Source

Lithium vapor pressure is not easily measured, since most measurement systems cannot be maintained at a temperature sufficient to prevent lithium condensation. However, an estimate of the lithium density can be made by using a known argon density in the source and measuring the ratio of $^7Li^+$ to Ar^+ ion peaks. A small amount of argon was in the discharge, but Ar^+ was not detected in Fig. 2(a), since the extraction energy was too high. If the extraction energy is lowered to allow the mass spectrometer to scan to higher masses, a small Ar^+ peak is noted, which is approximately two percent of the $^7Li^+$ ion peak (or 1.6% of the total beam), for an arc voltage of ~20 V. The ionization cross sections for atomic lithium and argon are well known and allow an estimate to be made of the lithium density in the ion source, if the argon density is known.

The argon pressure in the ion source has been measured with a barocell as about 5.0 mTorr without a discharge (giving a density of $\sim 1.6 \times 10^{14}$ cm^{-3}). When a discharge was present, the argon flow rate was

constant, implying that the product of argon neutral density and velocity is also constant. Therefore, the argon density during discharge operation (wall temperature ~673°K), corrected for the change in ion source temperature, was ~1.1×10^{14} cm^{-3}.

To determine the neutral lithium density, the ratio of lithium to argon ionization cross sections and ion velocities is needed. For an electron energy of 20 eV (primary electron energy), the ratio of cross sections is 7.6.[15] The velocity ratio is given by the inverse of the square root of the mass ratio. Hence, the percentage of argon ions in the ion source is 1.6% x $(40/7)^{1/2}$, or 3.8%. Correcting for the ionization efficiency, the neutral argon percentage is 3.8 x 7.6 or ~29%. The density of lithium would then be approximately 3.8×10^{14} cm^{-3}, which is equivalent to the equilibrium lithium density for a temperature of 850°K.

C. Negative Ion Species and Beam Current

Fig. 2(b) shows a mass spectrometer trace of the ion species in the extracted negative ion beam. Only Li^- ions (both $^6Li^-$ and $^7Li^-$) were detected. Under normal operation no H^- or O^- impurities were found in the extracted beam. Hence, the negative ion current measured by the Faraday cup was Li^- ions. As previously stated, measurements of the extracted negative ion current and the ratio of extracted electrons to negative ions were made with a permanent magnet mass separator and the Faraday cup. The maximum negative ion current measured was 14.9 μA (corresponding to a current density of 1.9 mA/cm^2) for a discharge voltage of 40 V and a discharge current of 4 A. Actual current densities could be higher, since no effort was made to improve the ion optics.

D. Plasma Density in the Ion Source

The extracted electron current measured by the mass separator was 3.75 mA, which gives an electron to ion ratio of 250 to 1 for the extracted beam. This ratio can presumably be improved when the magnetic filter geometry is optimized.[16] The extracted electron current measurement allows an estimate to be made of the plasma density in the extraction region of the ion source, if the electron temperature is known. Without probe measurements, this information is not available, but a good estimate can be obtained by using the electron temperature measured in similar hydrogen discharges, where T_e was found to have a value of 0.35 eV.[14] The density in the extraction region is given by:

$$n_e = 4I/(evA), \qquad (3)$$

where I is the electron current, e is the electronic charge, v is the thermal electron velocity $(8KT_e/\pi m_e)^{1/2}$, m_e is the electron mass, and A is the extraction area. Using the appropriate values for T_e, A, and I, an electron density of 3×10^{11} cm^{-3} is obtained. This is the extraction chamber plasma electron density.

III. Experiments with a Lithium Oven

In order to operate the ion source in steady state, a lithium oven was fabricated to maintain a constant neutral density in the ion source. The requirements for this oven are operation at high temperatures, up to 1300°K, small size, ease of lithium loading, and reasonable power consumption. Since the oven and ion source must be connected by some kind of lithium vapor transport pipe which restricts vapor flow, high oven

temperatures are required to drive sufficient vapor into the source to maintain a high neutral source density. The need for small size is due to the necessity for connecting the oven to the ion source, which itself is quite small. The oven, with a volume of ~8 cm^3, was of welded 314 stainless steel construction, as was the transport tube and radiation shielding. Electrical connections were made using stainless steel or tungsten wire. The oven was heated with heater wire that used an inner nichrome heating element surrounded by magnesium oxide electrical insulation and covered with a sheath made of inconel which was welded to the outside of the oven (see Fig. 3). The top of the oven was welded to the transport tube and bolted to the lower part of the oven. A nickel gasket formed a vapor seal to keep lithium from escaping at the joint. The transport tube was composed of two concentric tubes welded at the top. A current was passed through the tubes to electrically heat them to operating temperatures. When the copper vacuum housing of the oven assembly was connected to the ion source, the top of the transport tube fit into a hole in the heat shield of the ion source as shown in Fig. 3.

Temperature monitoring was provided by two alumel-chromel thermocouple junctions. One was spot welded to the base of the oven, and the other was spot welded to the inner transport tubing and insulated with quartz cloth. The oven and the transport tube had separate power supplies for independent temperature control, since the transport tube should be operated hotter than the oven in order to prevent lithium condensation. For operation at ~1270°K, the oven required about 180 W and the transport tube ~50 W of power.

Experiments using the lithium oven as the source of lithium for the ion source had very different results than those obtained by evaporating

lithium in the ion source. Fig. 4 (a) shows the output of the mass spectrometer when a positive ion beam is extracted from the ion source operating with an arc voltage of 80 V and an arc current of 3 A. The oven was maintained at a temperature of ~1100°K. The dimer ion fraction is less than two percent and the signal intensity is lower than previous results. Thus, both the neutral density in the ion source and the dimer fraction are likely to be low. This explains the very low Li^- ion output shown in Fig. 4 (b), when the source is operating at the same conditions except for an arc current of 2 A. With a low neutral density and a low dimer fraction, a low Li^- current density is observed as expected. However, the source could be operated in a steady state manner with the lithium oven.

With a low neutral density, the obvious remedy is to operate the lithium oven at higher temperatures in order to drive more lithium vapor into the ion source. However, as the temperature of the oven is raised over 1000°K, impurities are released from the oven assembly and drift into the ion source. Some of these impurities are seen in the negative ion mass spectrum of Fig. 4 (b). The impurity problem could presumably be corrected, however, the dimer fraction would still be unacceptably low. This indicates that dimers created by evaporation in the discharge are needed to achieve reasonable current densities.

IV. A MODEL FOR THE Li^- ION SOURCE

To model the filtered multicusp ion source for the case of a lithium discharge, a rate equation approach similar to that of McGeoch and Schlier[12] was taken. However, the dimer fraction will be inferred from experimental measurements, and modeled separately in a later section.

The electron collisional detachment process has been included, and a two-chamber system modeled rather than a single discharge region. With these modifications, the Li^- ion density and extracted current will be modeled for various discharge conditions.

A. Modelling of the First or Source Chamber

The first chamber contains the filament and hence high energy electrons, which are necessary for ionization and vibrational excitation. Therefore this chamber also has a relatively high electron temperature (T_e). Production of $Li_2(v^*)$ is assumed to be predominantly via electron collisions which result in electronically excited lithium molecules (Li_2^*) that radiatively decay into vibrationally excited states.

$$Li_2 + e^- \rightarrow Li_2^* + e^- \rightarrow Li_2(v^*) + e^- + h\nu \ . \qquad (4)$$

Wadehra and Michels have analyzed this process and find that electron energies of $1.8 < \varepsilon < 2.5$ eV should be suitable for populating high vibrational states.[17] To model this process, 10% of the electron population in the first chamber are assumed to be in this energy range, an assumption also made by McGeoch and Schlier. With this, reaction (4) proceeds with a rate constant of $k_e = 1.2 \times 10^{-8}$ $cm^3 s^{-1}$ for all electrons. Calculation of the rate constants is detailed in the Appendix.

$Li_2(v^*)$ is lost through wall collisions at a rate Ω, which is dependent on the ion source geometry, but for comparison with experimental results it is calculated to have a value of 1×10^5 s^{-1}. Wall collisions are assumed to completely de-excite $Li_2(v^*)$, since the sticking coefficient for lithium on surfaces is approximately unity by analogy with

sodium,[18] as was assumed by McGeoch and Schlier.[12] De-excitation via atomic lithium collisions proceeds as:

$$Li_2(v^*) + Li \rightarrow Li_2 + Li, \qquad (5)$$

with a rate constant k_r of $5x10^{-10}$ cm^3s^{-1}.[19]

Li^- ions are created via dissociative attachment as illustrated in equation (2). This process has a 'rate constant' k_D of $2x10^{-8}$ cm^3s^{-1} for low energy electrons.[20] The fraction of electrons with low energy, suitable for dissociative attachment, in the first chamber is designated S_1. S_1 is calculated by integrating a maxwellian electron distribution, with temperature T_e, from zero energy up to a limiting energy where k_D becomes small by analogy to hydrogen.

Li^- ions are lost by mutual neutralization

$$Li^- + Li^+ \rightarrow 2Li, \qquad (6)$$

and electron collisional detachment:

$$Li^- + e^- \rightarrow Li + 2e^- \ . \qquad (7)$$

Mutual neutralization proceeds with a rate constant k_M of $1.5x10^{-7}$ cm^3s^{-1}.[21] Electron collisional detachment, using a calculated cross-section for electron detachment,[22] proceeds with a rate constant k_d of $2.1x10^{-7}$ cm^3s^{-1} for an electron temperature of 1.4 eV. This may underestimate the actual rate constant, since the contribution of the primary electrons is ignored. Li^- ions are electrostatically confined by the positive plasma potential, and thus are not lost via wall collisions.

The negative ions created in the extraction region can gain random energy through several mechanisms, such as collisions with ions, locally

varying plasma potentials due to the magnetic field of the filter, or poorly optimized extraction from the ion source. These higher Li^- ion energies can be similar to the energies of the positive lithium ions in the discharge. Thus, for simplicity it will be assumed that the Li^- ions have the same translational energy as do Li^+ ions.

Using the rate constants for the above processes, rate equations for the $Li_2(v^*)$ and Li^- densities can be formulated. The neutral atomic and molecular lithium, $Li_2(v^*)$, electron, and Li^- densities are represented by n_1, n_2, n_2^*, n_e, and n^- respectively. For the vibrationally excited lithium molecules, a rate equation can be stated as,

$$dn_2^*/dt = k_e n_2 n_e - k_r n_2^* n_1 - k_D n_2^* n_e S_1 - \Omega n_2^*, \qquad (8)$$

while for negative lithium ions the equation becomes:

$$dn^-/dt = k_D n_2^* n_e S_1 - k_M n^-(n^- + n_e) - k_d n^- n_e \ . \qquad (9)$$

In equation 9 the positive ion density (n^+) is given by ($n^- + n_e$) through charge neutrality.

In steady-state operation and assuming spatially uniform conditions, the derivatives vanish and the equations can be solved for n_2^* in terms of n_1, n_2, n_e, and S_1; and for n^- in terms of n_e, n_2^*, and S_1. Solving for n_2^*, one arrives at:

$$n_2^* = (k_e n_2 n_e)/(k_r n_1 + k_D n_e S_1 + \Omega) \ . \qquad (10)$$

For n^-, the following equation is obtained:

$$n^- = (n_e/2)\{[A^2 + 4k_D n_2^* S_1/(k_M n_e)]^{1/2} - A\}; \qquad (11)$$

where $A = (1 + k_d/k_M)$. To calculate the extractable Li^- ion current density (J^-), the average velocity ($\underline{v}$) of the Li^- ions (calculated in the Appendix) is used:

$$J^- = qn^-\underline{v}/4, \qquad (12)$$

where q is the electronic charge. These equations apply for a single-chamber discharge.

B. Modelling of the Second or Extraction Chamber

The extraction chamber has a fundamental difference when compared to the first chamber, and that is the relative absence of energetic electrons. Measured electron temperatures in this region are quite low,[14] low enough to make rates of excitation, ionization, and detachment by electron impact negligible. In this chamber, the fast electron fraction is effectively zero. The rate equations for the second chamber are essentially the same as for the first chamber, with a few modifications. These include setting k_e and k_d to zero (no energetic electrons), and allowing the plasma density and electron temperature to change from their first chamber values. This approach is similar to, but less sophisticated, than the model developed by Hiskes[7,8] for modeling H^- ion sources. Since there is no volume source term for $Li_2(v^*)$, the rate equation becomes:

$$dn_2^*/dt = -k_r n_2^* n_1 - k_D n_2^* n_e S_2 - \Omega n_2^*, \qquad (13)$$

where S_2 is the fraction of the electron population with energies low enough for dissociative attachment. This results in an exponentially decaying n_2^* population along the axial (z) direction. Let v_2^* be the

average velocity of the excited molecules. By dividing both sides of equation (14) by v_2^* and integrating over z, an axial dependence of n_2^* can be determined.

$$n_2^*(z) = n_2^*(0)\ \exp[-(k_r n_1 + k_D n_e S_2 + \Omega)(z/v_2^*)] \quad . \quad (14)$$

In equation (14), z=0 represents the plane of the magnetic filter, and $n_2^*(0)$ is the bulk density at the edge of the filter in the first chamber. This is an approximation, since in this case we cannot expect a spatially uniform density of $Li_2(v^*)$ in the first chamber. For a given extraction chamber length, an average value of n_2^* can be calculated. This is given by:

$$<n_2^*> = n_2^*(0)\ (1/\Sigma z_{max})(1 - \exp(-\Sigma z_{max})), \qquad (15)$$

where Σ is $(k_r n_1 + k_D n_e S_2 + \Omega)/v_2^*$, and z_{max} is the length of the extraction region of the ion source. The negative ion density can now be solved to obtain:

$$n^- = (n_e/2)\{[1 + 4k_D<n_2^*>S_2/(k_M n_e)]^{1/2} - 1\}, \qquad (16)$$

where n_e is the electron density in the extraction region. These equations may now be used to calculate the extractable negative ion current from a discharge under a variety of conditions. The required input data are the atomic and molecular neutral densities and temperatures, the plasma density in both regions, and the electron temperature in both regions. In the next section, the single and tandem discharge systems will be compared and the effect of various discharge parameters on Li^- output will be explored.

C. Results for the Lithium Ion Source Model

The equations of the previous section were solved to yield extracted current densities for both the single and two-chamber (tandem) systems. As noted above, the plasma density and T_e for both chambers must be known in order to evaluate the equations. It has been observed experimentally that the plasma density in the extraction chamber is approximately a factor of five lower than in the first chamber for an ion source with a strong magnetic filter.[23] Therefore, only one plasma density needs to be specified. A first chamber electron density of 10^{12} cm^{-3} is assumed for most of the calculations. The measured electron temperatures of a low power filtered multicusp ion source, i.e. 1.4 eV in the first chamber and 0.35 eV in the second chamber, operating with hydrogen, are used as representative values.[14]

Other data needed to complete the solution are the neutral atomic lithium density (taken as 10^{15} cm^{-3} here), the percentage of lithium molecules in the neutral population (taken as 10% and further detailed in a later section), the wall temperature (taken from experimental data as 700°K and used for neutral velocity calculations), and the extraction chamber length (taken as 4 mm and used in the experiment). With a complete set of data, the scaling of Li^- current density with various parameters can be evaluated.

One of the most important parameters to ion source operation is the electron density in the source, since it roughly scales with the discharge power. In order to achieve the necessary current densities for fusion applications, ion sources will be scaled up in power density, with hopefully corresponding increases in negative ion density. Therefore, it is

important to evaluate the scaling of current density with the electron density. Fig. 5 is a graph of the Li^- current density as a function of the electron density in the first chamber (n_{e1}). The second chamber electron density (n_{e2}) is, as previously mentioned, taken to be $0.2n_{e1}$. Over the range of densities plotted, the Li^- current density for both single and two-chamber systems scales directly with electron density. Only when the negative ion loss terms, such as mutual neutralization, become comparable to the dissociative attachment term, will the scaling saturate. Saturation is hinted at in Fig. 5 by a very slight droop in the current density plot at the highest electron densities. That is due to the onset of mutual neutralization, and will ultimately cause the current density to saturate, but at extreme electron densities. The plasma density scaling is very favorable for improved operation at higher discharge power.

The fraction of Li_2 in the neutral population is expected to be a critical parameter in the lithium ion source. In equilibrium, the fraction of Li_2 in lithium vapor is very small (typically one percent or less). In nonequilibrium evaporation or supersonic expansion, the percentage of molecules can be very high (greater than ten percent).[24] Fig. 6 is a plot of the Li^- current density as a function of the molecular fraction. As expected, the current density for both the single and two-chamber systems increases with the percentage of Li_2 in the ion source. The single chamber system exhibits a linear relationship with the molecular percentage, while the two-chamber system encounters a slight saturation effect as higher percentages are reached. However, these higher percentages are unlikely to be achieved in a steady-state system.

Another important experimental variable is the neutral density in the source. Low neutral densities are preferred, in order to reduce stripping of the negative ions outside of the source and in the accelerator. Unfortunately, best results in terms of current density are usually obtained with high gas densities in the ion source. The extracted current density as a function of the atomic lithium density is plotted in Fig. 7. The behavior of the single and two-chamber systems are distinctly different as the density is increased. The current density in a single chamber system initially increases rapidly until saturation sets in at about $5x10^{14}$ cm^{-3}. Saturation is due to the de-excitation of the molecules by collisions with atoms. Likewise, the two-chamber system output decreases after peaking at about $5x10^{14}$ cm^{-3}. Since the electron density is lower in the second chamber, the atomic de-excitation rate overtakes the dissociative attachment rate as the neutral density is increased. This effect is amplified in the two-chamber system due to the exponential decay of the excited molecule population with distance from the filter.

The second-chamber electron temperature is also an important parameter for negative-ion production in the two-chamber system. Although the measured T_e is very low for strongly filtered systems (0.35 eV), Fig. 8 shows that further decreases in T_e could provide substantial increases in Li^- current density. The increase is due to the peaking of the dissociative attachment cross-section for very low energy electrons. If T_e is allowed to increase, a steady drop in current density results. The first chamber electron temperature only affects the two-chamber system output by changing the negative ion temperature in the second chamber. However, the current density in a single chamber system will decrease

substantially for higher T_e, due to the reduction in the density of electrons with the proper energy for dissociative attachment, and increased electron collisional detachment of Li^-.

These results show the advantage of the two-chamber system versus a single-chamber discharge. Higher current densities are obtained by the tandem system because there is no loss of Li^- by electron collisional detachment. As expected, the electron density, molecular fraction, and second chamber electron temperature are extremely important parameters. Both the electron density and molecular fraction should be increased as much as possible. The second chamber T_e should be minimized, which can be accomplished with a stronger filter, but at a cost of some electron density in the second chamber. The use of a tandem discharge configuration also allows a lower optimum pressure than a single-chamber discharge, which becomes important when stripping of the negative ion beam outside of the source is considered.

In addition to maximization of the negative ion current density, the minimization of the number of electrons extracted from the ion source is of considerable importance. These electrons increase the requirements on extraction and acceleration power supplies, cause stripping of the beam, add to space charge in the beam, create additional heat loading on the extraction and acceleration electrodes, and can increase voltage breakdown problems in high voltage structures. Therefore, the extracted electron current should be reduced as much as possible. The tandem geometry provides a large improvement over the single-chamber system in this respect as well. Not only is the electron density in the extraction region substantially reduced, but the T_e of these electrons is also much

lower. This results in about an order of magnitude reduction in the extracted electron current density for the tandem configuration.

Useful Li^- current densities appear achievable with the tandem discharge geometry. Current densities of several mA/cm^2 can be produced in the optimized two-chamber ion source. The most critical factor in these calculations has been the assumption of a relatively high molecular fraction, ~10%, which was inferred from experimental observations. The following section will model the Li_2 surface formation process in order to determine how molecules are predominantly formed and whether the 10% figure can be explained and possibly improved.

D. Model for Dimer (Li_2) Formation in the Ion Source

Previous results show the importance of achieving a high dimer fraction of the neutral species in the ion source. For lithium vapor in thermal equilibrium, dimer fractions are limited to less than two percent for vapor pressures of interest.[25] The dimer fraction increases with evaporation rate, i.e. the liquid surface temperature, but a practical limit is reached when Li^- ion stripping by neutral particle collisions becomes significant. Source pressures greater than 0.1 Torr are thus not feasible. Increasing the dimer fraction will therefore require a nonequilibrium approach to dimer formation.

There are several methods to create high dimer fractions in alkali metal vapors. One of the best known is to use a high temperature oven to produce a vapor at high pressure which is expanded through a supersonic nozzle, the approach advocated by McGeoch and Schlier.[12] The drawback to this method is that the lithium vapor makes only one pass through the ion source before it must be collected and piped back to the oven. An

alternative method, which does not require the use of an external oven, is to allow lithium evaporation from a very restricted area of the wall of the ion source.

If the temperature of the ion source wall is allowed to vary significantly with position, the local evaporation rate will also vary strongly with position. Thus, the effective area for lithium evaporation can be greatly reduced by making most of the ion source wall relatively cold ($T_{wall} < 750°K$). The local rate of evaporation of the hotter regions of the wall must be increased to compensate, since all surfaces contribute to lithium condensation. A high local evaporation rate is conducive to higher rates of dimer formation. The picture of the source now is one where most of the wall is cold and acts as a sink for lithium vapor. The lithium condensate moves to a hotter region where it evaporates under conditions favorable for dimer formation.

There are two mechanisms to passively transport the lithium condensate to the hot region. One is to use gravity to move a thin ($< 10^{-4}$ m) film of condensate to the bottom of the ion source where a hot region is located. The second is to use the natural tendency of lithium adsorbates (submonolayer) to spread out in order to minimize surface concentration.[26] However, this second approach is unlikely to be feasible since the colder walls of the ion source will undoubtedly have a multiple monolayer (ML) lithium coverage due to the high rate of condensation. Hence, transport via gravity of a thin film of lithium condensate is the mechanism assumed here.

To model this situation, a small fraction of the ion source wall area will be assumed hot and the rest relatively cold. The cold region has a negligibly small evaporation rate, but lithium condenses on these surfaces

and is transported to the hot region. The hot region is where the vast majority of lithium is vaporized due to higher temperatures. Since the sticking coefficient of lithium is approximately unity, any lithium atom or molecule which collides with a wall surface is removed from the vapor phase. Steady state operation requires that the rate of condensation on all wall surfaces be balanced by evaporation from the hot region. This section develops rate equations for these processes with the goal of finding a practical way of significantly enhancing the dimer fraction in the ion source.

To determine the condensation rate, the neutral species will be assumed to have a maxwellian velocity distribution at a gas temperature equal to the temperature of the hot wall surface, while the gas density is left as a free variable to be given later. The rate of condensation (in atoms) can then be given as:

$$R_{con} = (n_1 v_1 + 2n_2 v_2)A/4, \qquad (17)$$

where v_1 is the average velocity of the lithium atoms, v_2 the average velocity of the dimers, and A is the wall area of the ion source.

The rate of atomic desorption is given by:[27]

$$R_{de1} = K_1 m, \qquad (18)$$

where m is the surface concentration of lithium atoms, and K_1 is a rate constant which is approximately given by:

$$K_1 \approx (2\pi kT/h)\exp(-E_a/kT), \qquad (19)$$

where k is Boltzmann's constant, h is Planck's constant, and E_a is the adsorption energy of a lithium atom on the wall surface. The molecular desorption rate (in atoms) is given by:[27]

$$R_{de2} = K_2 m^2, \qquad (20)$$

where K_2 is given by:

$$K_2 \approx S_m(2\pi kT/h)^2(\pi MkT)^{1/2}(p_2/p_1{}^2)\exp(-2E_a/kT), \quad (21)$$

where S_m is the molecular sticking coefficient (also approximately unity), M is the atomic mass of lithium, and p_1 and p_2 are the equilibrium partial pressures of the atomic and molecular vapor respectively.

In order to evaluate these expressions, values for E_a, p_1, p_2, and m are required. E_a is a function of m in the low coverage limit and has been measured for lithium on tungsten,[28] since no other similar data are available, a tungsten wall surface will be modeled in all calculations. Values of p_1 and p_2 have been tabulated as a function of temperature.[25] Given this information, the atomic and molecular desorption rates can be calculated. The dimer fraction of the ion source will be evaluated as a function of the temperature of the hot wall surface and the corresponding fractional area where evaporation takes place. The adsorption energy is taken as 1.56 eV (Ref. 28) for a one-monolayer coverage of lithium on tungsten. This coverage is near optimal for dimer production since lower coverages have a higher adsorption energy.

E. Results for the Dimer Model

Fig. 9 is a plot of the percentage of lithium evaporating in the form of molecules, as a function of the temperature of the hot wall area, for a

neutral lithium density of 10^{15} cm^{-3}. As the temperature is increased, the evaporation rate rises steeply. In order to maintain a fixed density, the fraction of the hot wall surface is decreased to balance the evaporation and condensation rates. This is shown in Fig. 10 where the hot wall temperature is plotted against the fractional hot area. These results indicate that the optimal situation is to minimize the hot wall area, and use the highest temperature that maintains at least one ML coverage of lithium on the tungsten surface. Dimer fractions of greater than 10% seem feasible without exotic lithium plumbing and at reasonable source neutral densities.

V. COMPARISON OF THEORY AND EXPERIMENT FOR Li^- ION PRODUCTION

With the experimental parameters calculated previously, a comparison between the theoretical model of the lithium ion source and experiment can be made. The experimental parameters were an electron density $3x10^{11}$ cm^{-3} in the extraction chamber (or $1.5x10^{12}$ cm^{-3} in the first chamber for the model), a dimer fraction of 12.3%, a neutral lithium density of $3.8x10^{14}$ cm^{-3}, and an extraction chamber length of 4 mm. The electron temperatures for both regions used in the model will again be used for comparison. A model calculation using these parameters gives an extracted Li^- current density of 1.6 mA/cm^2 for a tandem discharge. This is in close agreement with the experimental value of 1.9 mA/cm^2. It should be noted that this experimental value of Li^- current density is the best achieved, and not an average.

If the filter magnets are removed from the ion source, a single-chamber results. The model predicts approximately a factor of four decrease in Li^- current density. Experimentally, the Li^- ion output drops

to a negligible value without the presence of the magnetic filter. This implies that the model may in fact be underestimating the electron collisional detachment rate, which did not include the contribution of primary electrons. This results in an overestimate of the single-chamber Li^- output, but does not affect the tandem discharge results. The single-chamber result is consistent with the assumption of dissociative attachment as the dominant Li^- ion formation mechanism.

VI. CONCLUSION

The results of experiments on a small multicusp Li^- ion source show that reasonable current densities for diagnostic applications are easily achieved. It remains to extend this result to steady state operation in a source with a larger usable extraction area. Key areas for improvement are control of liner temperature to improve and maintain a high dimer fraction and supply of lithium to the ion source. However, there are no outstanding technical problems involved in doing so. It also appears, using the ion source model, that a substantial improvement in Li^- current density can be achieved with increases in the plasma and dimer density. Thus Li^- ion sources suitable for diagnostic applications can be achieved with only modest additional development.

ACKNOWLEDGEMENTS

We would like to thank Prof. W. B. Kunkel and Prof. D. Olander for fruitful discussions and D. Moussa for technical assistance. This work is supported by AFOSR (under Contract No. AFOSR-ISSA-88-0003), and the Director, Office of Energy Research, Office of Fusion Energy, Development

and Technology Division, of the U.S. Department of Energy under Contract No. DE-AC03-76SF00098.

APPENDIX RATE CONSTANTS FOR THE LITHIUM ION SOURCE MODEL

This appendix details how the values of the various rate constants and other constants were evaluated. The 'rate constant' (k_d) for the dissociative attachment (D.A.) reaction (Eq. 2) is simply that given by McGeoch and Schlier without modification.[12] However, it should be noted that this 'rate constant' considers only low energy electrons (< 0.5 eV). Consequently, it is multiplied by a factor (S_1 or S_2) denoting the fraction of electrons with energies less than 0.5 eV. These factors are calculated by evaluating the fraction of electrons in this energy range for a maxwellian distribution of a specified electron temperature.

The vibrational excitation of the lithium molecule by electron impact (Eq. 4) has been analyzed by Wadehra and Michels.[17] The rate constant for this reaction (k_e) was also computed by McGeoch and Schlier.[12] Their rate constant included only the exothermic vibrational states for dissociative attachment. For H^-, the dissociative attachment cross section is also very large for endothermic states such as $v = 6$-9.[29] For lithium, the vibrational state equivalent to the $v = 6$ state in hydrogen was considered as the lowest state of importance for D.A. The equivalent state was determined by multiplying the threshold electron energy for D.A. in $H_2(v^* = 6)$ (1.0 eV), by the ratio of the molecular binding energies (1.06 eV/4.52 eV). This gives an equivalent threshold energy for the lithium system (0.23 eV), which corresponds to an energy just above $v = 5$ in lithium. Hence, all vibrational states from 6 on up are used to model the D.A. reaction for lithium. The rate constant (k_e), given by McGeoch and

Schlier, was then multiplied by the sum of the cross sections for vibrational excitation of Li_2 to states from 6 on up (given by Wadehra and Michels), and divided by the sum of the cross sections of the states used by McGeoch and Schlier (10 on up). This gives a factor of 2.4 increase in the excitation rate constant used by McGeoch and Schlier ($5x10^{-9}$) resulting in $k_e = 1.2x10^{-8}$ cm^3s^{-1}.

Loss of vibrationally excited lithium molecules via wall collisions is given by a frequency $\Omega = 2x10^5/a$ cms^{-1}, where a is a characteristic dimension of the ion source.[12] This is simply used with a source dimension of 2 cm to obtain $\Omega = 1x10^5$ s^{-1}.

De-excitation of vibrationally excited lithium molecules by collisions with atoms (Eq. 5) proceeds with a rate constant k_r of $1x10^{-9}$ cm^3s^{-1} given by McGeoch and Schlier. This rate constant assumes complete de-excitation in a single collision. However, it is known that this process involves a statistical sharing of energies and that the lithium molecule on average retains 50-60% of the total energy as internal energy.[19] Considering that lithium atoms have some energy (~0.1 eV for evaporation at 1100 °K), and that the internal energy of $Li_2(v^*)$ is ~0.4 eV (v = 10), it appears that the internal energy lost by this process is small. As a conservative estimate, two collisions will be assumed effective in de-exciting $Li_2(v^*)$, which cuts the above rate constant in half and gives $k_r = 5x10^{-10}$ cm^3s^{-1}.

Li^- ions can be lost by mutual neutralization (Eq. 6) and by electron collisional detachment (Eq. 7). Mutual neutralization proceeds with a rate constant k_M of $1.5x10^{-7}$ cm^3s^{-1}.[21] This rate constant has not been modified from that used by McGeoch and Schlier. Detachment is important when energetic electrons are present. The cross section for this reaction

is large[22] and results in a rate constant k_d of 2.1×10^{-7} $cm^3 s^{-1}$ for an electron temperature of 1.4 eV.

The velocities ascribed to the excited molecules and negative ions are important in order to calculate the average $Li_2(v^*)$ density in the second-chamber, and the extracted Li^- current density respectively. The $Li_2(v^*)$ molecules are assumed to be in thermal equilibrium with the hot part of the wall surface of the ion source. This is reasonable since the hot part of the wall is the source of Li_2, and because of the short lifetime of Li_2 due to the high wall collision rate. The $Li_2(v^*)$ velocity ($\underline{v}$) is then calculated by computing the average velocity of a maxwellian distribution of Li_2 at the wall temperature. In reality, the actual temperature of the $Li_2(v^*)$ molecules is not known, but the wall temperature is a good approximation. The Li^- velocity is calculated in the same manner using the first chamber electron temperature as a representative value for the ion temperature.

REFERENCES

1 K. H. Berkner, R. V. Pyle, and J. W. Stearns, Nucl. Fusion 15, 249 (1975).

2. L. R. Grisham, D. E. Post, and D. R. Mikkelsen, Nuc. Technol. Fusion, 3, 121 (1983).

3. W. P. West, Rev. Sci. Instrum. 57, 2006 (1986).

4. W. P. West, D. M. Thomas, J. S. deGrassie, and S. B. Zheng, Phys. Rev. Lett., 58, 2758 (1987).

5. W. P. West, D. M. Thomas, E. S. Ensberg, J. S. deGrassie, and J. F. Baur, Rev. Sci. Instrum. 57, 1552 (1986).

6. S. R. Walther, *Development of H^- and Li^- Ion Sources*, Ph. D. Thesis, University of California at Berkeley, 1989, also Lawrence Berkeley Laboratory Report No. 26618, Jan. 1989.

7. J. R. Hiskes and A. M. Karo, J. Appl. Phys., 56, 1927 (1984).

8. J. R. Hiskes, A. M. Karo, and P. A. Willman, J. Appl. Phys., 58, 1759 (1985).

9. J. R. Hiskes, Comments At. Mol. Phys., 19, 59 (1987).

10. K. N. Leung and W. B. Kunkel, Phys. Rev. Lett. 59, 787 (1987).

11. S. R. Walther, K. N. Leung, and W. B. Kunkel, Appl. Phys. Lett., 51, 566 (1987).

12. M. W. McGeoch and R. E. Schlier, J. Appl. Phys., 61, 4955 (1987).

13. K. W. Ehlers, K. N. Leung, and M. D. Williams, Rev. Sci. Instrum. 50, 1031 (1979).

14. K. N. Leung, K. W. Ehlers, and M. Bacal, Rev. Sci. Instrum. 54, 56 (1983).

15. C. F. Barnett, et. al., *Atomic Data for Controlled Fusion Research*, Oak Ridge National Laboratory, ORNL-5206, (1977).

16. K. N. Leung, K. W. Ehlers, and R. V. Pyle, Rev. Sci. Instrum. 56, 321 (1985).
17. J. M. Wadehra and H. H. Michels, Chem. Phys. Lett., 114, 380 (1985).
18. J. P. Woerdman and S. S. Eskildsen, Chem. Phys., 65, 83 (1982).
19. J. C. Whitehead, Mol. Phys., 29, 177 (1975).
20. M. W. McGeoch and R. E. Schlier, Phys. Rev. A, 33, 1708 (1986).
21. B. M. Smirnov, *Negative Ions*, Chapter 5, McGraw Hill, 1982, New York.
22. Udit Narain and N. K. Jain, Can. J. Phys., 53, 1221 (1975).
23. K. N. Leung, private communication.
24. E. Schumacher, W. H. Gerber, H. P. Harri, M. Hofmann, and E. Scholl, *Metal Bonding and Interactions in High Temperature Systems*, Section 8, 83, American Chemical Society Symposium 179, Washington D. C. 1982.
25. A. N. Nesmeyanov, *Vapor Pressure of the Chemical Elements*, Elsevier Publishing Company, New York,1963.
26. D. L. Doering and S. Semancik, Surf. Sci., 175, L730 (1986).
27. Gert Ehrlich, J. Chem. Phys. 31, 1111 (1959); and D. Olander, private communication.
28. V. K. Medvedev and T. P. Smereka, Sov. Phys. Solid State, 16, 1046 (1974).
29. J. M. Wadehra and J. N. Bardsley, Phys. Rev. Lett., 41, 1795 (1978).

Figure Captions

Fig. 1 A schematic diagram of the lithium ion source.

Fig. 2 Mass spectrometer signal showing the the beam species for (a) the positive ion beam and (b) the negative ion beam.

Fig. 3 A schematic diagram of the lithium oven and ion source.

Fig. 4 Mass spectrometer signal showing the the beam species for (a) the positive ion beam and (b) the negative ion beam when operating with the lithium oven.

Fig. 5 A plot of the Li^- current density as a function of the first chamber electron density

Fig. 6 A plot of the Li^- current density as a function of the percentage of lithium vapor in the form of molecules.

Fig. 7 A plot of the Li^- current density versus the atomic lithium density

Fig. 8 A plot of the Li^- current density as a function of the second chamber electron temperature

Fig.9 A plot of the percentage of lithium neutral particles evaporated as molecules versus the temperature of the hot wall surface.

Fig. 10 A plot of the fractional hot area of the wall surface required to maintain a constant neutral density as a function of the temperature of that surface.

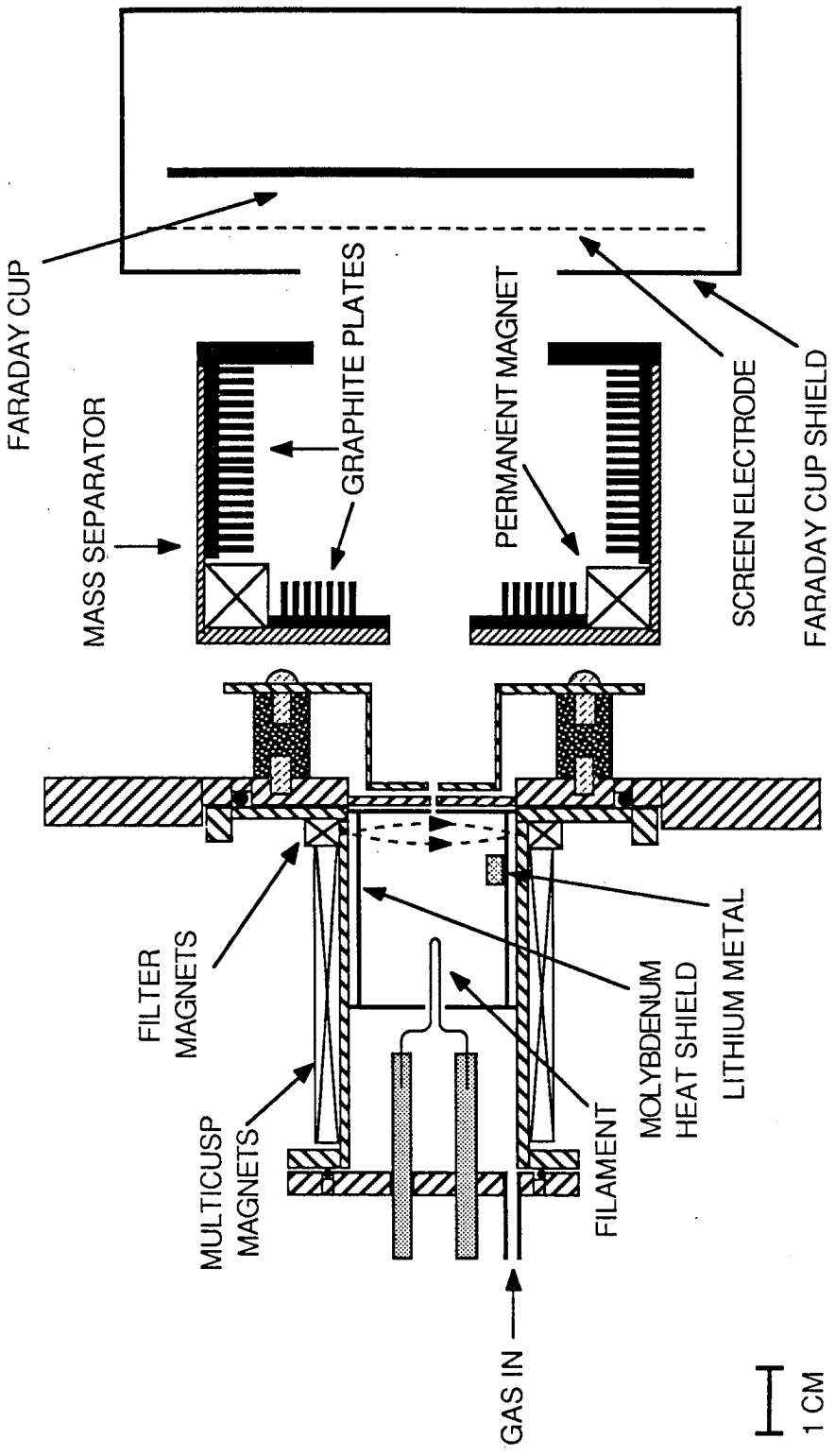

XBL 874-1775

Figure 1.

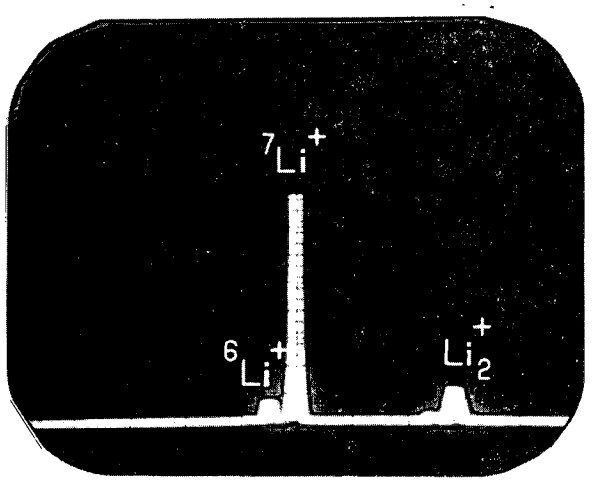

(a)

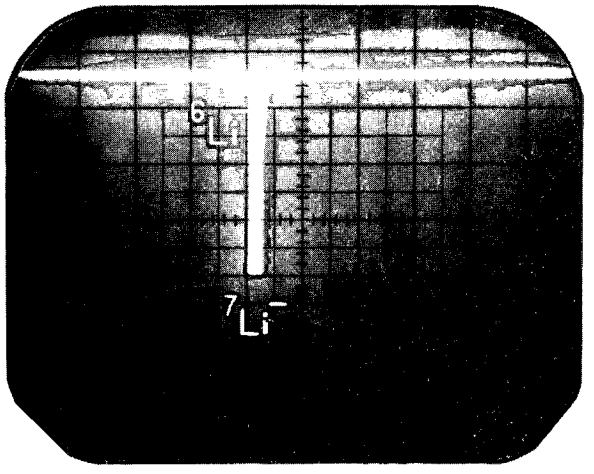

(b)

XBB 874-3134

Figure 2.

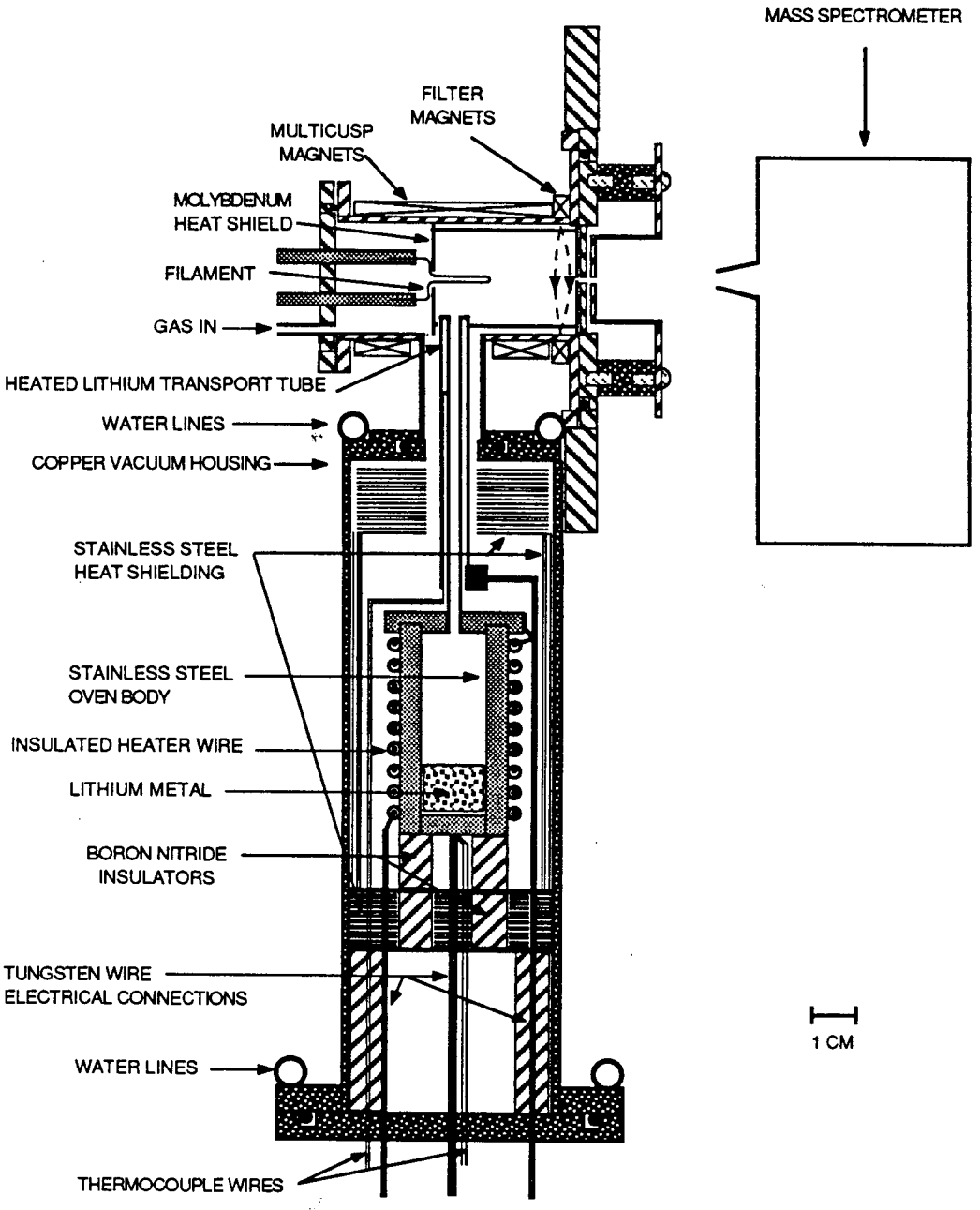
MASS SPECTROMETER
FILTER MAGNETS
MULTICUSP MAGNETS
MOLYBDENUM HEAT SHIELD
FILAMENT
GAS IN
HEATED LITHIUM TRANSPORT TUBE
WATER LINES
COPPER VACUUM HOUSING
STAINLESS STEEL HEAT SHIELDING
STAINLESS STEEL OVEN BODY
INSULATED HEATER WIRE
LITHIUM METAL
BORON NITRIDE INSULATORS
TUNGSTEN WIRE ELECTRICAL CONNECTIONS
WATER LINES
THERMOCOUPLE WIRES
1 CM
XBL 892-415

Figure 3.

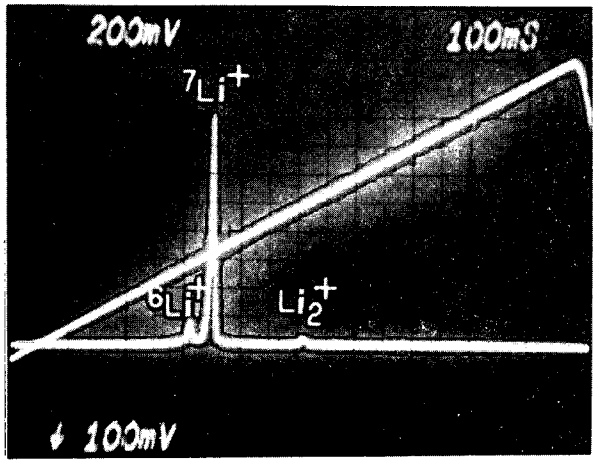

(a)

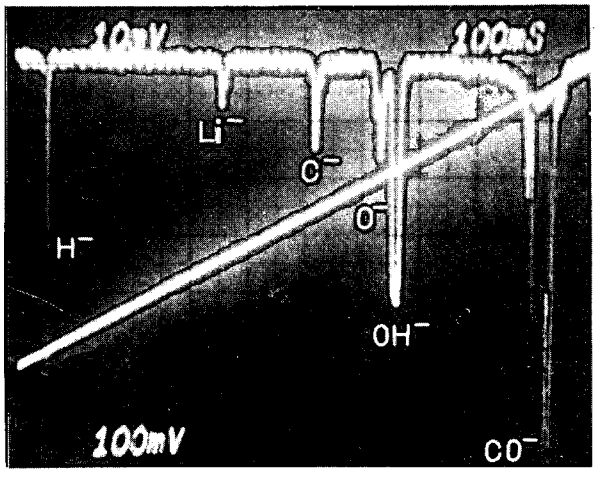

(b)

XBB 880-10624

Figure 4.

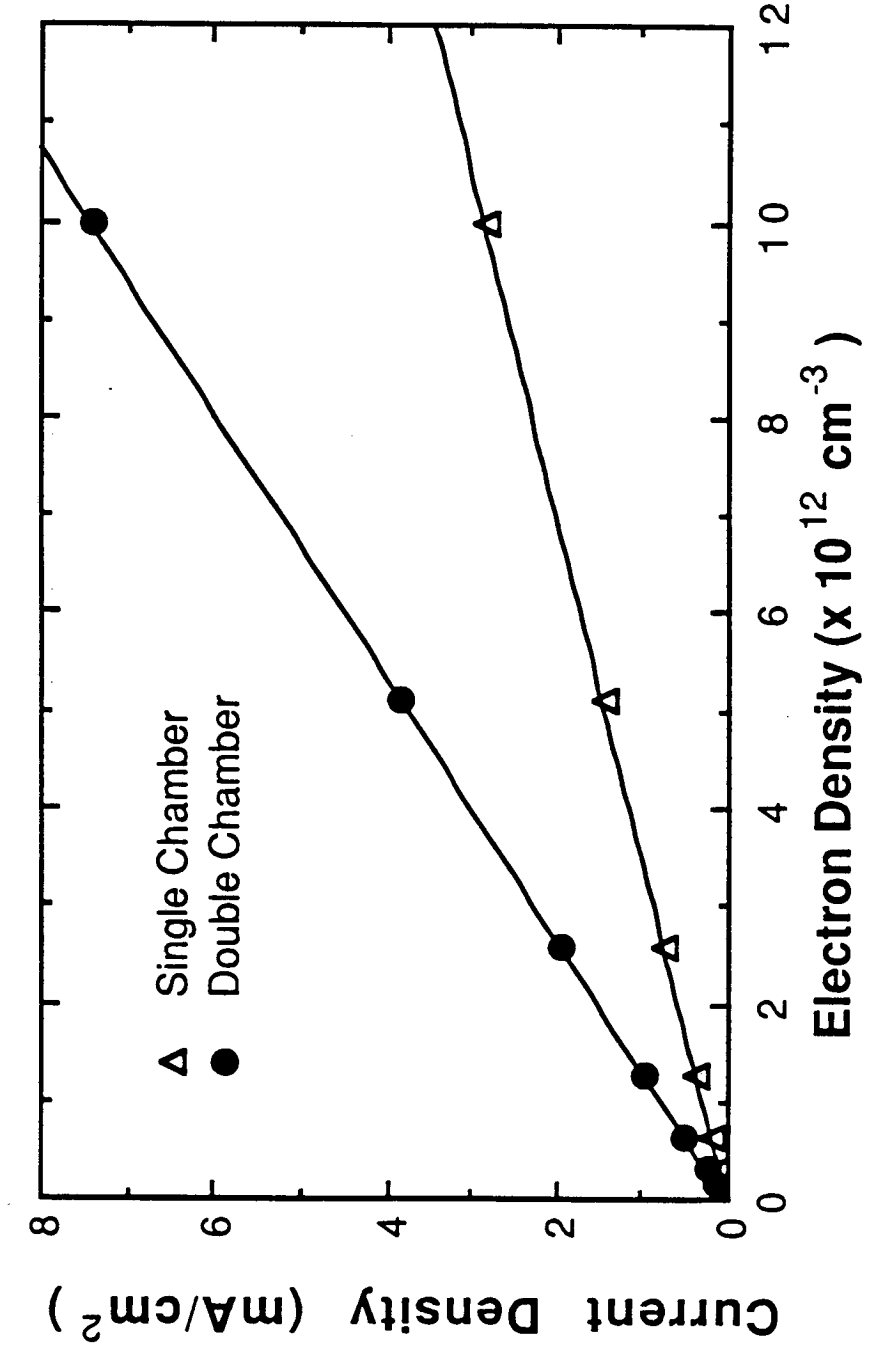

XBL 892-416

Figure 5.

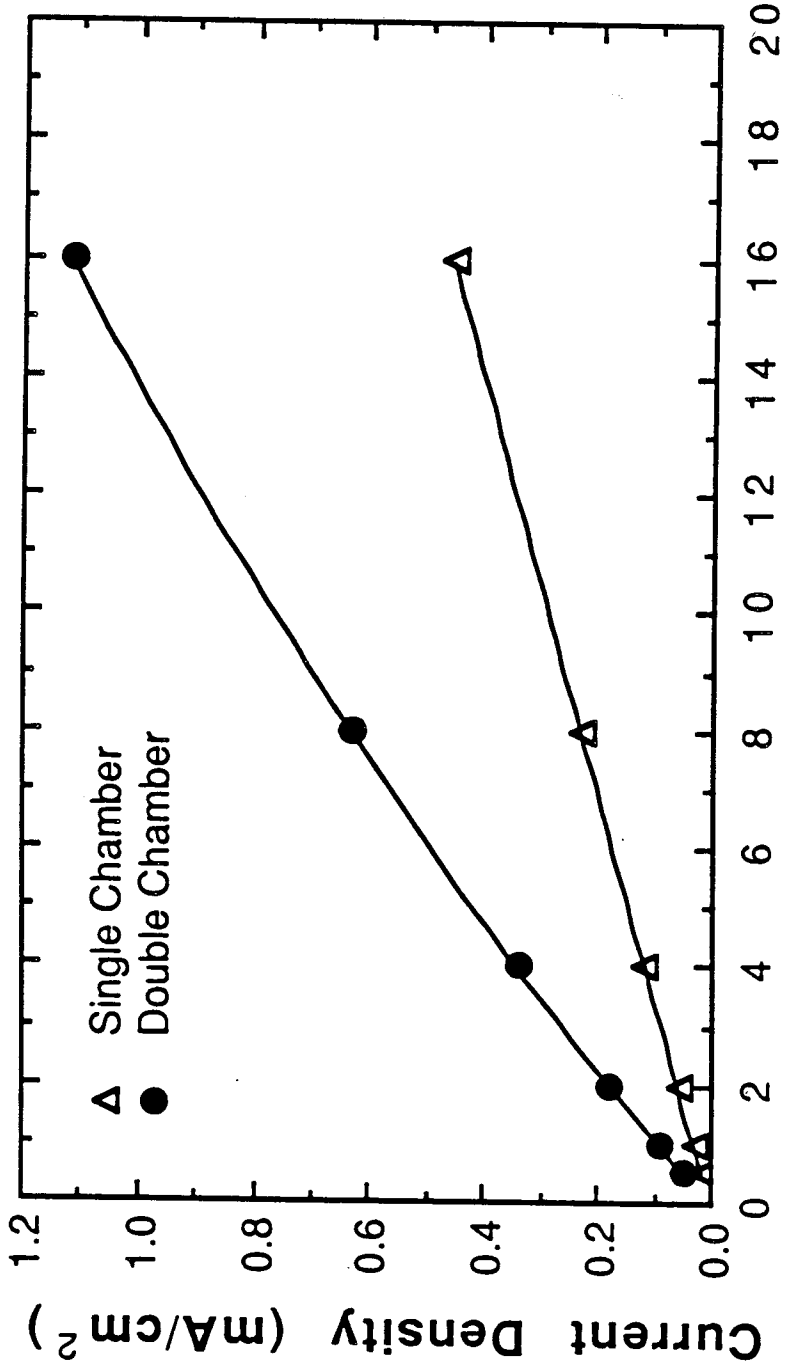

XBL 892-417

Figure 6.

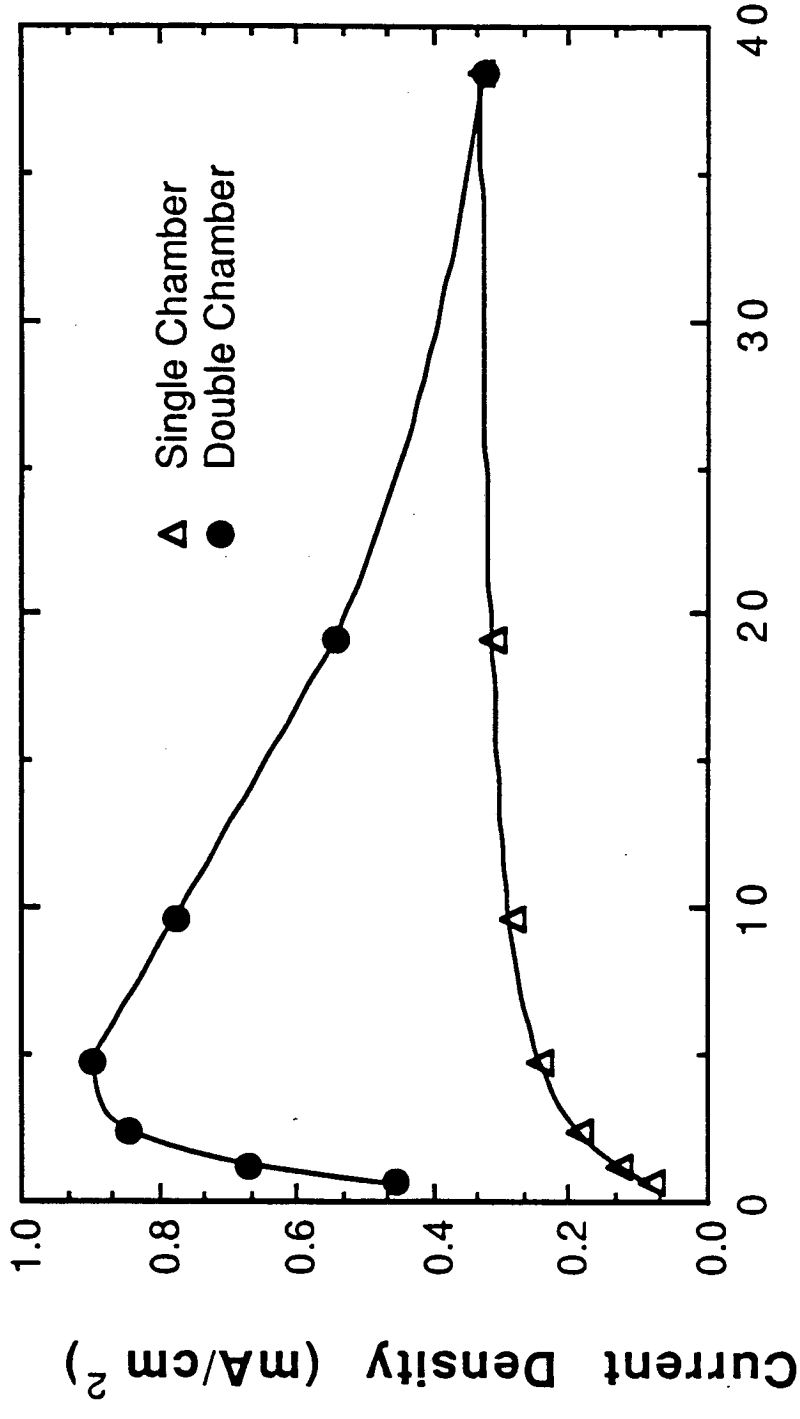

XBL 892-418

Figure 7.

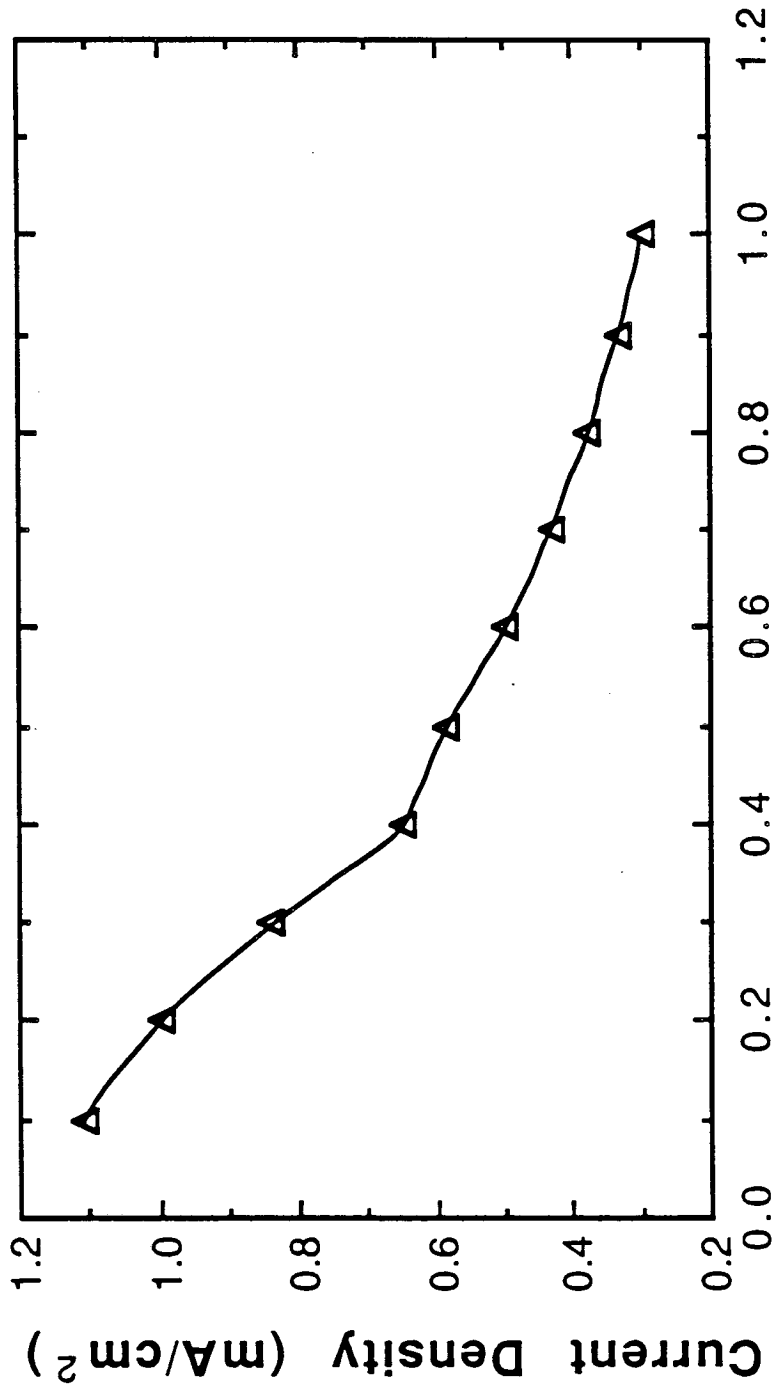

XBL 892-419

Figure 8.

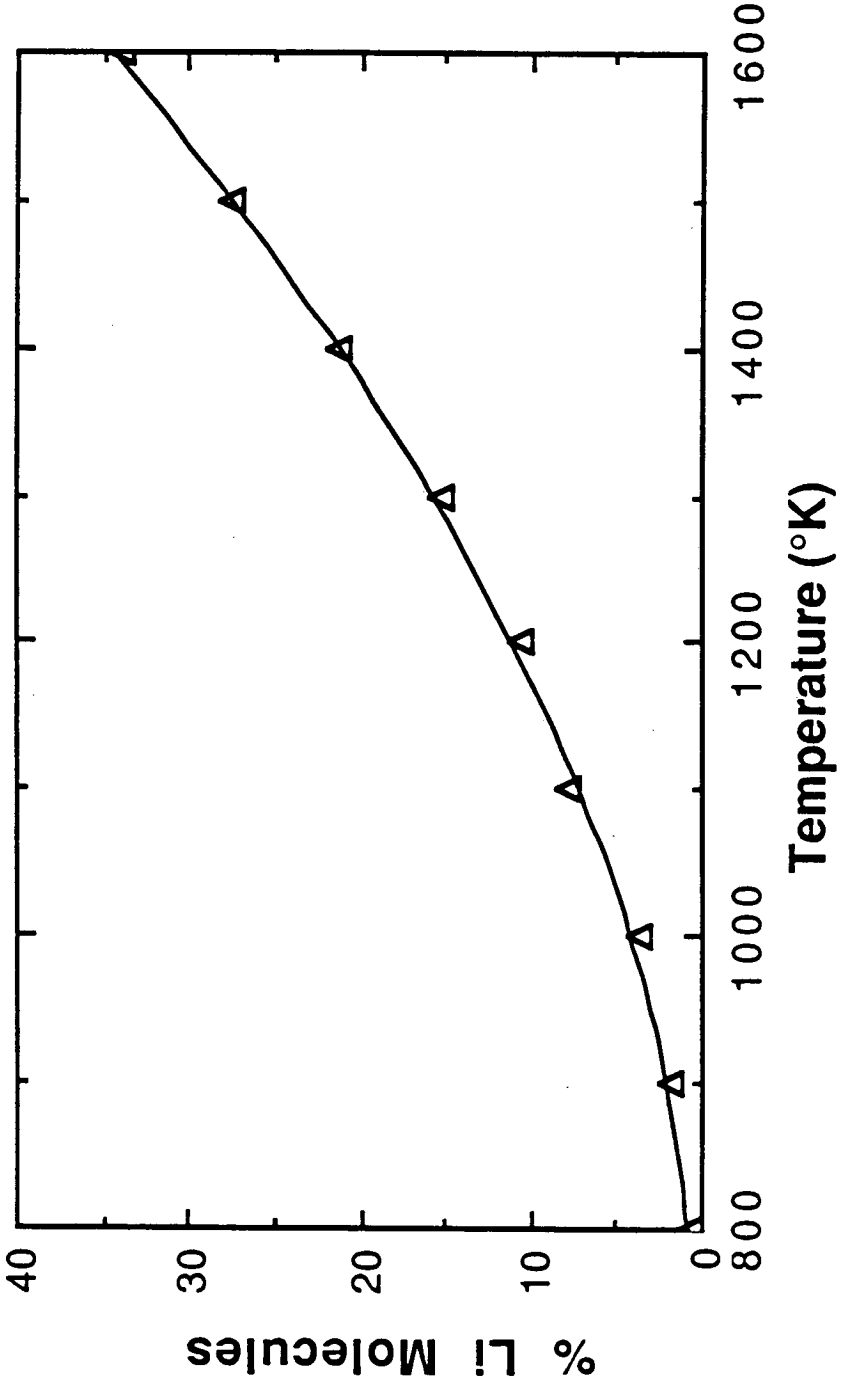

XBL 892-420

Figure 9.

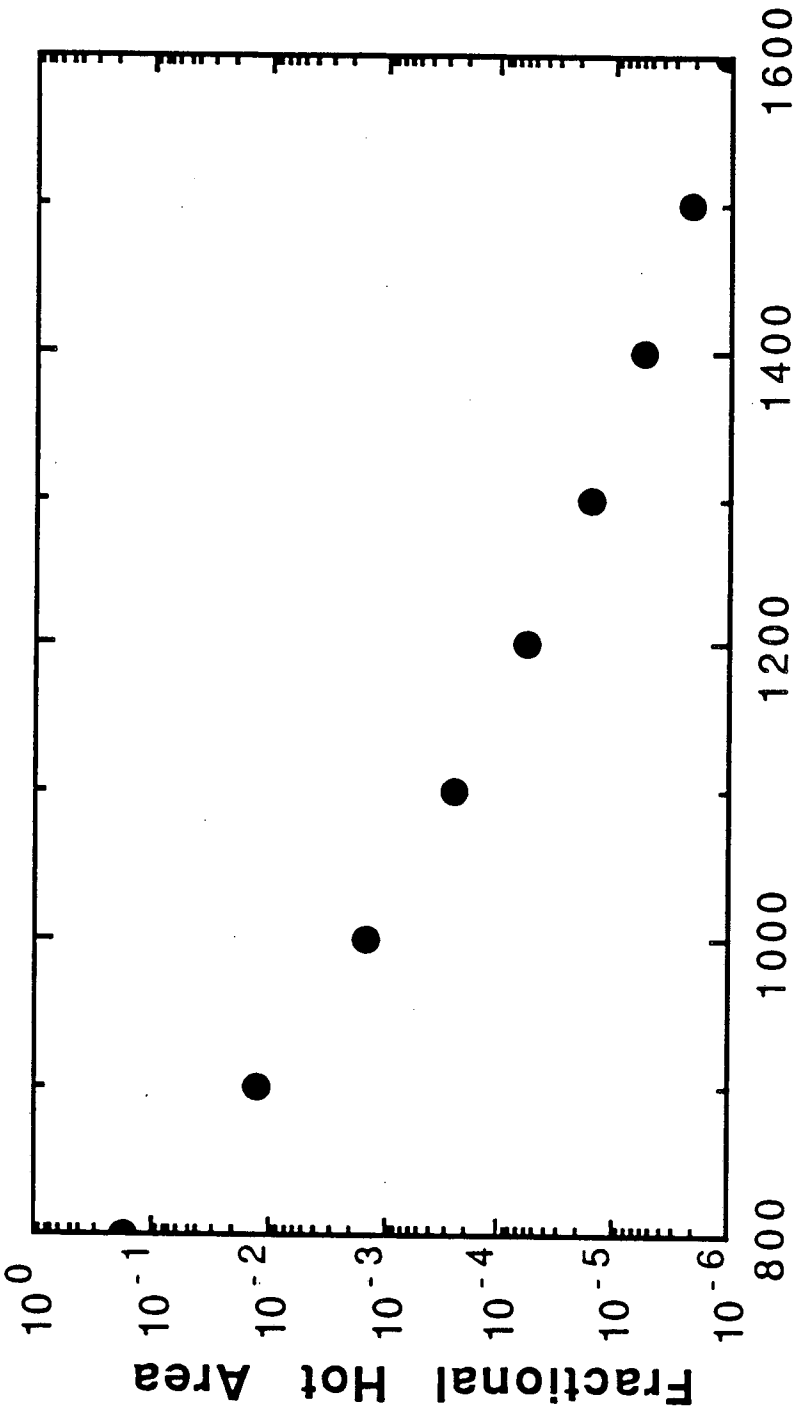

XBL 892-421

Figure 10.

LAWRENCE BERKELEY LABORATORY
TECHNICAL INFORMATION DEPARTMENT
1 CYCLOTRON ROAD
BERKELEY, CALIFORNIA 94720